SupraCells: Living Mammalian Cells Protected within Functional Modular Nanoparticle-Based Exoskeletons

Wei Zhu[a,b,*,‡], Jimin Guo[b,‡], Shahrouz Amini[c], Yi Ju[d], Jacob Ongudi Agola[b], Andreas Zimpel[e], Jin Shang[f], Achraf Noureddine[b], Frank Caruso[d], Stefan Wuttke[e], Jonas G. Croissant[b,*], C. Jeffrey Brinker[b,*]

Abstract: Creating a synthetic exoskeleton from abiotic materials to protect delicate mammalian cells and impart them with new functionalities could revolutionize fields like cell-based sensing and create diverse new cellular phenotypes. Herein, we introduce the concept of 'SupraCells', which are living mammalian cells encapsulated and protected within functional modular nanoparticle-based exoskeletons. Exoskeletons are generated within seconds through immediate interparticle and cell/particle complexation that abolishes the macropinocytotic and endocytotic nanoparticle internalization pathways that occur without complexation. SupraCell formation was shown to be generalizable to wide classes of nanoparticles and various types of cells. It induces a spore-like state, wherein cells do not replicate or spread on surfaces but are endowed with extremophile properties, e.g., resistance to osmotic stress, reactive oxygen species, pH, and UV exposure, along with abiotic properties like magnetism, conductivity, and multi-fluorescence. Upon de-complexation cells return to their normal replicative states. SupraCells represent a new class of living hybrid materials with

[a] Prof. W. Zhu
School of Biology and Biological Engineering, South China University of Technology, 382 East Outer Loop Road, University Park, Guangzhou 510006 (P. R. China)
E-mail: zhuw200461170@163.com;
[b] Prof. W. Zhu, J. Guo, Dr. J. O. Agola, Prof. J. G. Croissant, Prof. C. J. Brinker
Center for Micro-Engineered Materials, Department of Chemical and Biological Engineering, the University of New Mexico, Albuquerque, New Mexico 87131 (USA)
E-mail: jonascroissant@unm.edu; jbrinker@unm.edu;
[c] Dr. S. Amini
Max Planck Institute of Colloids and Interfaces, Am Mühlenberg 1, 14476 Potsdam (Germany)
[d] Dr. Y. Ju, Prof. F. Caruso
ARC Centre of Excellence in Convergent Bio-Nano Science and Technology and the Department of Chemical and Biomolecular Engineering, The University of Melbourne, Parkville, Victoria 3010 (Australia)
[e] Dr. A. Zimpel, Prof. S. Wuttke
Department of Chemistry and Center for NanoScience (CeNS), University of Munich (LMU), Butenandtstraße 11, 81377 Munich (Germany)
[f] Prof. J. Shang
School of Energy and Environment,
City University of Hong Kong, Tat Chee Avenue, Kowloon, Hong Kong SAR (P. R. China)
[‡] These authors contributed equally to this work.
Supporting information for this article is given via a link at the end of the document.

a broad range of functionalities.

Enhancing or augmenting the performance of mammalian cells could result in new classes of smart responsive living materials. Mammalian cells exhibit complex functionalities like sensing, signal transduction, and protein expression, but they remain fragile and highly susceptible to intracellular and extracellular stressors.[1] So far, to impart delicate mammalian cells with greater cellular durability, such as enhanced resistance against UV, freezing, and enzymatic attack, *etc*., a series of coating strategies/nanotechniques have been developed to encapsulate single living cells within protective nanostructured films or shells.[2] For example, Akashi and co-workers employed layer-by-layer (LbL) assembly to encapsulate mouse L929 fibroblast cells and demonstrated control of the cell surface microenvironment and cellular functions.[3a] Hawker and Soh reported a surface-initiated controlled radical polymerization method to encapsulate human Jurkat cells within poly(ethylene glycol) acrylate copolymer coatings and demonstrated manipulation of the cell phenotypes and underlying cellular processes.[4] Choi and co-workers reported a bioinspired mineralization process to encapsulate mammalian cells within inorganic coatings (e.g., silica, titania, or hybrid silica-titania). The encapsulated cells exhibited enhanced resistance to freezing, malnutrition, and showed a potential use in T-Cell therapy applications.[5] Quite recently, Choi further demonstrated cellular encapsulation within supramolecular (Fe^{III})/tannic acid (TA) coordination complexes which exhibited on-demand degradation properties.[6] Finally, Yang and co-workers highlighted the phase-transitioned lysozyme (PTL) coating on yeast cell by pure proteins, which may be further extended to mammalian cell systems to enrich the coating strategy pools.[7] Despite the above advances in cellular encapsulation approaches, the thin film coating methodologies employed to date and properties of the resultant films possess in general several limitations. First because the coating procedures are often time consuming

(e.g. LBL) and conducted in the presence of living cells,[3] the synthetic conditions of precursor chemistry, pH, temperature, solvent, and reaction time are always limited to those exhibiting high biocompatibility. This necessarily excludes many classes of materials from being candidates for cellular encapsulation. Second, the synthetic procedures employed provide little control of the permeability of the coating (e.g. silica nanoshells).[5] Permeability toward nutrients, metabolites, and signaling molecules is vital to maintaining cellular viability and functionality. Finally, current most coating procedures do not provide a versatile means to develop combined/integrated multi-functionalities.[8] These limitations necessitate the development of a new cytoprotective encapsulation strategy.

Synthetic nanoparticles (NPs) with various chemical compositions and diverse functionalities naturally interact with mammalian cell surfaces through multiple non-covalent binding interactions developed with proteins and other cellular membrane components.[9] Often these interactions lead to NP accumulation and subsequent internalization by phagocytosis or macropinocytosis based on membrane extension or invagination and wrapping of individual or groups of nanoparticles.[10] The natural coherence of the NP/cellular membrane interface suggests that NPs might be ideal candidates for cellular encapsulation if accompanying NP internalization mechanisms could be suppressed. Here, we describe a general means of uniform cellular encapsulation within a NP-based exoskeleton employing arbitrary NP building blocks (and combinations thereof) and inter-nanoparticle ligands (Figure 1A). This simple universal encapsulation approach, referred to here as ‘SupraCells’, instantly encapsulates living mammalian cells within functional, modular, NP-based exoskeletons avoiding typical endocytotic nanoparticle internalization pathways. It provides an ability to endow the encapsulated cell with useful, tunable physico-chemical properties (e.g., optical, magnetic, and sensing properties) depending on the NPs or NP combinations (Figure 1B). The

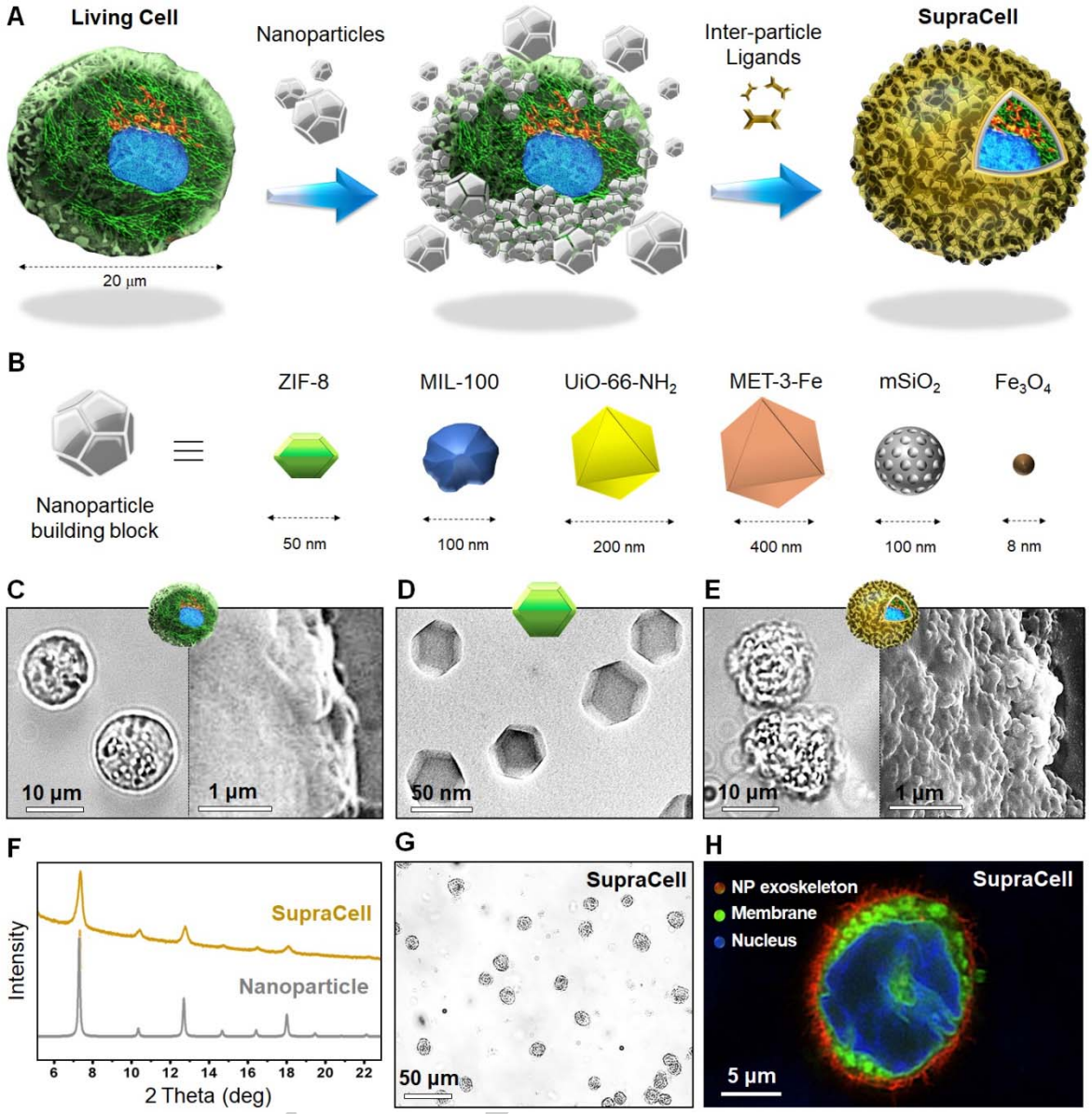

Figure 1. **Formation and characterization of SupraCells**. (**A**) Schematic representation of SupraCell formation via immediate, self-limiting ligand assisted formation of NP exoskeletons that 'freeze' natural mammalian endocytotic pathways. (**B**) Representation of various NP building blocks including MOFs (ZIF-8, MIL-100, UiO-66, MET-3-Fe), mesoporous silica ($mSiO_2$), and iron oxide (Fe_3O_4) NPs. (**C**) Bright field (left) and scanning electron microscopy (right) images of HeLa cells. (**D**) Transmission electron image of ZIF-8 nanobuilding blocks. (**E**) Bright field (left) and scanning electron microscopy (right) images of HeLa SupraCells based on ZIF-8 nanobuilding blocks and tannic acid inter-particle ligands. (**F**) X-ray diffraction pattern of Supra-HeLa Cell-ZIF-8 and ZIF-8 NPs. (**G**) Low-magnification bright field image of Supra-HeLa Cell-ZIF-8. (**H**) Z-stack confocal image of a SupraCell demonstrating the homogeneous formation of the NP-based exoskeleton (red-colored from rhodamine labeled ZIF-8 NPs).

potential chemical diversity of SupraCells is enormous, and here we demonstrated SupraCell prototypes prepared with NP-exoskeletons including metal-organic frameworks (MOFs) (i.e., ZIF-8, MIL-100, UiO-66-NH_2, MET-3-Fe types, vide infra), mesoporous silica NPs ($mSiO_2$ and dye-labeled $mSiO_2$), iron oxide (Fe_3O_4) NPs (Figure 1B) and NP combinations. SupraCell formation maintains normal cellular functions (e.g., viability, metabolism) but induces a spore-like state, wherein cells do not replicate or spread on surfaces but are endowed with extremophile properties, e.g., resistance to osmotic stress, reactive oxygen species (ROS), pH, and UV exposure. NP functionality confers to the cell abiotic properties including tunable cell-mechanics, selective permeability, intracellular activity sensing, multi-fluorescence, magnetism, and electrical conductivity, which are utterly foreign to the native mammalian cells.

As a first demonstration of the SupraCell concept, individual HeLa cells encapsulated within ZIF-8 (zeolitic imidazolate framework-8) NP-based exoskeletons (termed Supra-HeLa Cell-ZIF-8) were constructed via the sequential addition of a colloidal ZIF-8 solution and tannic acid to cell suspensions prepared in PBS solution (see materials and methods in SI for detailed information). The ca. 50 nm diameter, well-defined rhombic dodecahedral shape, and cubic $I\bar{4}3\,m$ group symmetry of water borne colloidal ZIF-8 NPs were confirmed using transmission electron microscopy (TEM) and wide-angle X-ray diffraction (XRD) analyses (Figure 1D,F). Only thirty seconds of incubation were necessary to freeze the cellular internalization of the ZIF-8 nanobuilding blocks via tannic acid-mediated interparticle binding due to strong-multivalent metal-phenolic complexation.[11] The formation of the NP-based exoskeleton surrounding the HeLa cells is driven by the multitude of NP-cell membrane and NP-NP interactions achieved naturally and via the multidentate tannic acid complexation. We directly visualized the NP exoskeleton using bright field and scanning electron microscopy (SEM) imaging of both normal cells and SupraCells (Figure 1C,E; Figure S1). Fourier-transform

infrared spectroscopy performed on Supra-HeLa Cell-ZIF-8 confirmed the coordination of tannic acid to zinc open sites on the ZIF-8 surface, as evidenced by the characteristic peaks at 1179 and 994 cm^{-1} assigned to the vibration of C=N and C−N in the imidazole ring of ZIF-8 and 1083 cm^{-1} assigned to the stretching vibration of C-O in tannic acid (Figure S2), respectively. Analyzing nearly one hundred SupraCells on bright field and SEM images strongly supported the fact that all individual HeLa cells had homogeneous conformal exoskeletons (Figure 1G; Figure S3), as further confirmed by confocal scanning laser microscopy (CLSM) of a rhodamine-labeled ZIF-8-NP-based exoskeleton (Figure 1H), where we observe a coherent, conformal ZIF-8-NP layer encapsulating the HeLa cell. Wide-angle XRD (Figure 1F) along with energy-dispersive X-ray (EDX) spectroscopy mapping of zinc, carbon, and oxygen atoms (Figure S4) confirmed preservation of the structural and chemical integrity of the ZIF-8-NP exoskeletons.[12] The generality of the NP-based exoskeleton paradigm was then demonstrated on other mammalian cell lines including A549 cells (adenocarcinomic human alveolar basal epithelial cell) and HL-60 cells (human promyelocytic leukemia cells), both yielding SupraCells-ZIF-8 with continuous exoskeletons (Figure S5-6). We note that the NP concentration and ratio of NPs to the tannic acid complexation agents affect the coating uniformity and integrity. To demonstrate this we employed bright and hydrolytically very stable Alexa Fluor 647-labeled MSN@ZIF-8 hybrid NPs (Figure S7) to prepare Supra-HeLa Cells-MSN@ZIF-8, wherein the concentration of tannic acid was maintained at 16 μg/mL and the MSN@ZIF-8 hybrid NP concentration was increased from 10 to 160 μg/mL. Figure S8 show the corresponding confocal microscopy images of the resultant SupraCells following three cycles of washing to avoid any physical adsorption. Clearly, when the NP concentration is low (10-60 μg/mL) (Figure S8A-C), no NPs can be detected after washing whereas we observe a discrete distribution of NPs around the cell surface without

washing (Figure S9). This indicates that for low (sub-monolayer) NP concentrations, there is insufficient NP-NP complexation to form a coherent, stable, conformal coating. With the increase of the NP concentration to 100 µg/mL, a continuous, conformal NP-based exoskeleton could be obtained (Figure S8D) and confirmed to be stable after the same washing conditions, indicating the importance of the continuity of NPs to maximize NP-NP complexation and strengthen the cellular exoskeleton. With a further increase of NP concentration to 160 µg/mL, no difference was observable compared to the NP concentration of 100 µg/mL (Figure S8E). We attribute this to saturation of the tannic acid binding sites, disallowing further binding of NPs.

We then sought to demonstrate the versatility of the SupraCell approach by extending it to different nanobuilding blocks for multifunction integration. Additional types of MOF NPs (e.g. MIL-100(Fe), UiO-66-NH_2, MET-3-Fe) with different framework-related functionalities (e.g. sensing, and conductivity), $mSiO_2$ and dye-labeled $mSiO_2$, as well as magnetic Fe_3O_4 NPs were selected for SupraCell exoskeleton formation experiments employing HeLa cells. For every case, successful preparation of NP was confirmed by a panel of analyses including XRD, SEM, TEM, and dynamic light scattering (DLS) (Figure S10-14). For the different NP systems, we used different inter-particle ligand chemistries to form the exoskeletons via inter-nanoparticle binding at the cellular interface, namely, tannic acid for MOF systems based on metal-phenolic interactions,[11] 1,4-benzendiboronic acid for phenol-functionalized $mSiO_2$ or Fe_3O_4,[13] exploiting boronate-phenolic interactions, and 4-arm-PEG5K-SH for thiol-modified $mSiO_2$ through thiol-thiol reactions[14] (Figure S15). We then successfully extended these SupraCell syntheses to different cell lines (e.g., Raw 264.7 cell lines, see detailed synthesis in Supplementary Section S4 and Scheme S1). Based on characterization by SEM, optical microscopy, and CLSM, all SupraCell constructs depicted continuous, conformal NP-based

exoskeletons (Figure S16-19). As a control without inter-nanoparticle crosslinking, the NPs were quickly (< 5 min) physically adsorbed onto the cellular surface and then internalized by the cell and accumulated around the nucleus (Figure S20). However, after the construction of NP-based exoskeletons, the NPs internalization could be further blocked (Figure S21). The robustness and versatility of our approach using various mammalian cell lines and nanobuilding blocks hence strongly suggests that a vast library of SupraCells can now be designed for a wide array of scientific investigations.

Implicit in the SupraCell concept of protecting cells within NP exoskeletons is preservation of cellular function. In order to assess the cytocompatibility of the SupraCell process, we determined the viabilities of HeLa-, A549-, Raw 264.7-, and HL-60-based SupraCell suspensions using the CellTiter-Glo® 2.0 cell viability kit. All the SupraCells exhibited cell viabilities of at least 90% (Figure S22), indicating negligible cytotoxicity of the exoskeleton formation process. Note that due to the fast formation of the cell exoskeleton in seconds, there may be a very small portion of NPs especially at the outer layer of the exoskeleton that could detach from the exoskeleton because of insufficient binding interactions and then be taken up by the encapsulated cells (or other cells). However, due to the low toxicity of the NPs (Table S1), the cell viability affected by these very small portions of NPs should be minimal. Further extending the incubation times up to 72 h reduced the viability in an identical manner to that of native HeLa cells maintained in suspension (Figure 2A). Here it should be noted that normally adherent cells maintained in suspension, which lose their cell–extracellular matrix (ECM) interactions, undergo a process of anoikis where the cell cycle is arrested and a specific form of caspase-mediated programmed cell death (apoptosis) occurs.[15]

Having established Supracell viabilities, we next examined the related biological behaviors. We hypothesized that the expected rigidity (*vide infra*) of the NP exoskeleton, cellular isolation,

and obscuration of cell adhesion molecules like integrins would conspire to arrest cellular adhesion, spreading, and proliferation. To test this hypothesis, we evaluated the proliferation of HeLa based SupraCell-ZIF-8 suspensions when introduced to glass substrates under standard culture conditions at time points ranging from 1-24 h post exoskeleton formation and compared it to that of native HeLa cells. As shown in Figure S23, unlike native HeLa cells, SupraCells do not adhere, spread or proliferate. However, based on the reversibility of metal-phenolic complexation, exposure of SupraCell-ZIF-8 to ethylenediaminetetraacetic acid solution (EDTA, 20 mM, pH 5.0) for 30 min results in Zn chelation, complete exoskeleton removal, and recovery of native HeLa cell behavior. Note that this kind of disassembly or dissociation process only took place at high EDTA concentration. Under the low concentration of EDTA that was the same as the one in Trypsin-EDTA (0.25%) solution, which was used for

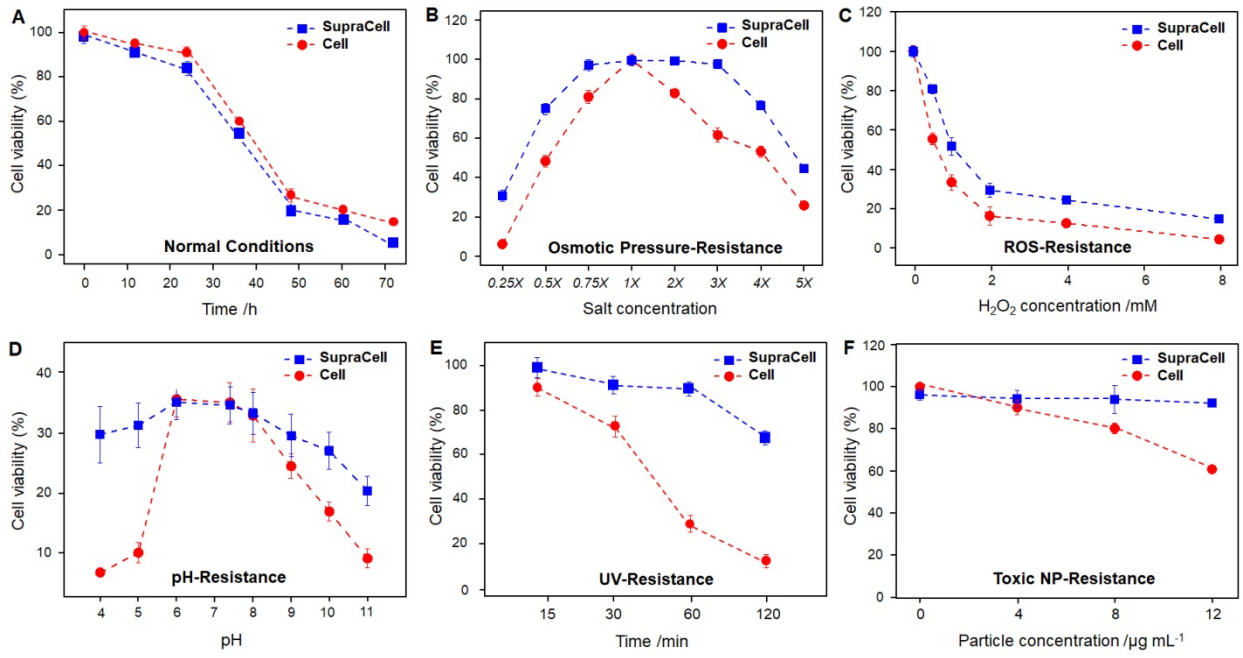

Figure 2. Enhanced resistance of SupraCells against endo- and exogenous stimuli. (**A**) Viability of HeLa cells versus corresponding SupraCells based on MIL-100(Fe) nanobuilding blocks, in normal conditions. (**B**) Viability of HeLa cells versus SupraCells-MIL-100(Fe) as a function of the salt concentration (i.e. osmotic pressure stimulus), (**C**) H_2O_2 concentration (i.e. ROS stimulus), (**D**) pH, (**E**) UV irradiation time (254 nm), and (**F**) toxic silver NPs (diameter: ~5.0 nm).

cell detachment from the culture plate, no NP disassembly occurred (Figure S24). Figure S25 shows the formation and removal of ZIF-8 or MIL-100(Fe) exoskeletons had a negligible effect on viability compared to native control cells. As shown in Figure S26, after the removal of exoskeleton, HeLa cells can again adhere, spread, and proliferate under cell culture conditions. Analysis of proliferation rates indicate that the 'reversed' SupraCells have almost the same proliferation rate compared to native cells (Figure S27-28). This on-demand exoskeleton formation and degradation capability confers to the mammalian cells behaviors normally associated with the germination of natural spores.

In order to demonstrate how the SupraCell exoskeletons protect the cells against external stressors, SupraCell-MIL-100(Fe) was exposed to various osmotic pressure, pH, reactive oxygen species (ROS), UV stressors, and toxic NPs (Figure 2). First upon exposure to varying ionic strength solutions (expressed as x PBS, where 1x PBS is isotonic with living cells), native HeLa cells show 100% viability at 1x PBS but greatly reduced viability at lower or higher osmotic stress and only 6.4% and 26.0% viability at 0.25x PBS and 5x PBS, respectively. In comparison SupraCell-MIL-100(Fe) shows nearly 100% viability from 0.75x PBS to 3x PBS and cell viabilities of 31.0% and 44.7%, at 0.25x PBS and 5x PBS, respectively. In mammalian cells, hypertonic conditions result in water expulsion from cells and cell shrinkage, while hypotonic conditions result in cell swelling, both processes resulting in rapid cell lysis for conditions other than isotonic (Figure S29A-C). The enhanced mechanical stiffness and membrane reinforcement provided by the SupraCell exoskeleton (*vide infra*) resists both cellular shrinkage and swelling processes, as shown in Figure S29D-F, thereby greatly reducing cell lysis under hypotonic and hypertonic conditions.

Second, ROS can cause oxidative damage and produce adverse modification to cellular components (e.g. lipids, and DNA).[16] As shown in Figure 2C, the viabilities of SupraCells

paralleled but were statistically greater than those of native HeLa cells in the presence of increasing hydrogen peroxide (H_2O_2) concentrations. The increased ROS-resistance of SupraCells may be associated with the unique antioxidant properties of tannic acid in the exoskeleton nanostructure.[17] Third, the viability of SupraCells was tested over the pH range 4-11 as it is known that altered acid-base balance and extreme pH ranges can disrupt cell metabolic processes and cause irreversible cell damage.[18] As shown in Figure 2D, pH values below 6.0 or greater than 8.0 led to an abrupt decrease of viability for native HeLa cells, whereas SupraCells showed increased resistance toward pH variation and exhibited two-fold and three-fold higher viabilities at pH 11 and 4, respectively. We attribute this pH resistance to the ion chelating effect resulting from the porous exoskeleton framework.[19] Note that in an attempt to show the difference between cells and Supracells, the referred to experiment was performed at 37˚C in 1X PBS. At this higher temperature, the metabolic rate of cells increases, resulting in a greater synthesis and degradation rate of biomolecules. Because the experiment is performed at 1X PBS without cell culture media, biomolecule degradation results in a continuous decrease of cell viability for both blank cells and Supracells. Fourth, we determined the resistance of SupraCells to UV irradiation (λ = 254 nm, 4W) in comparison to native mammalian cells. As expected, UV exposure caused a sharp decline in the survival of native cells after 60 min, resulting in about 30% survival,[20] whereas SupraCells remained largely unaffected after the same exposure time (Figure 2E and Figure S30). After two hours of UV exposure, the viability of SupraCells was over six times higher than the native cells. We attribute the UV resistance to the high UV-absorption coefficient of the MIL-100(Fe)-based SupraCell exoskeletons over the wavelength range 200–300 nm (Figure S31). Furthermore, the intrinsic porosity of MIL-100(Fe) enables loading of UV-absorbing dyes (e.g. Congo red) in the exoskeleton further enhancing the protection of SupraCell-MIL-100 against UV irradiation

(Congo red-loaded SupraCell-MIL-100(Fe) SupraCells exhibited 15% greater viability upon exposure to 365 nm UV light for 120 min compared to unloaded SupraCells) (Figure S32). The ability to load molecular cargos into the MOF exoskeleton opens vast possibilities to tune the properties of SupraCells. Finally, both native cells and SupraCells were exposed to cytotoxic silver (Ag) nanoparticles (diameter: ~5.0 nm) at different concentrations. As shown in Figure 2F, native cells were very sensitive to toxic Ag NPs and showed a dose-dependent response behavior. On the contrary, Supracells exhibited ~100% viability even at high concentrations of 12 μg/mL, highlighting the excellent protection conferred by the NP-based exoskeletons.

The mechanical behavior of MOF-based SupraCells was determined by nano-indentation and compared to native cells (see Figure 3A). HeLa-based SupraCell-ZIF-8 and SupraCell-MIL-100(Fe) samples along with native HeLa cells were subjected to multiple loading-unloading cycles to differing contact depths (Figure S33). Due to the size and softness of the cell samples, a Berkovich tip with wide contact angle (142.3°) was used. Extracted loading-unloading curves (Figure S33) revealed that the contact depths for the SupraCells were ~50% lower than the contact depths of native HeLa cells, indicating the higher stiffness afforded by the exoskeletons. Slopes of the loading-unloading curves were then used to determine the stiffness *S* and elastic modulus *E* as a function of contact depth (Figure S34). Figure 3B compares *S* and *E* for SupraCells and native HeLa cells indented to a contact depth of 100-nm (the approximate thickness of the exoskeleton) where we find SupraCells to have 2-4 times greater stiffness and modulus, explaining in part their greater resistance to osmotic stress. ZIF-8 and MIL-100(Fe)-based SupraCells were also found to have differing contact depth dependencies of their elastic moduli (Figure S34), whereby, MIL-100(Fe) is a flexible MOF that can exhibit densification under applied pressure while ZIF-8- based SupraCells are not based on flexible nanostructures.[21]

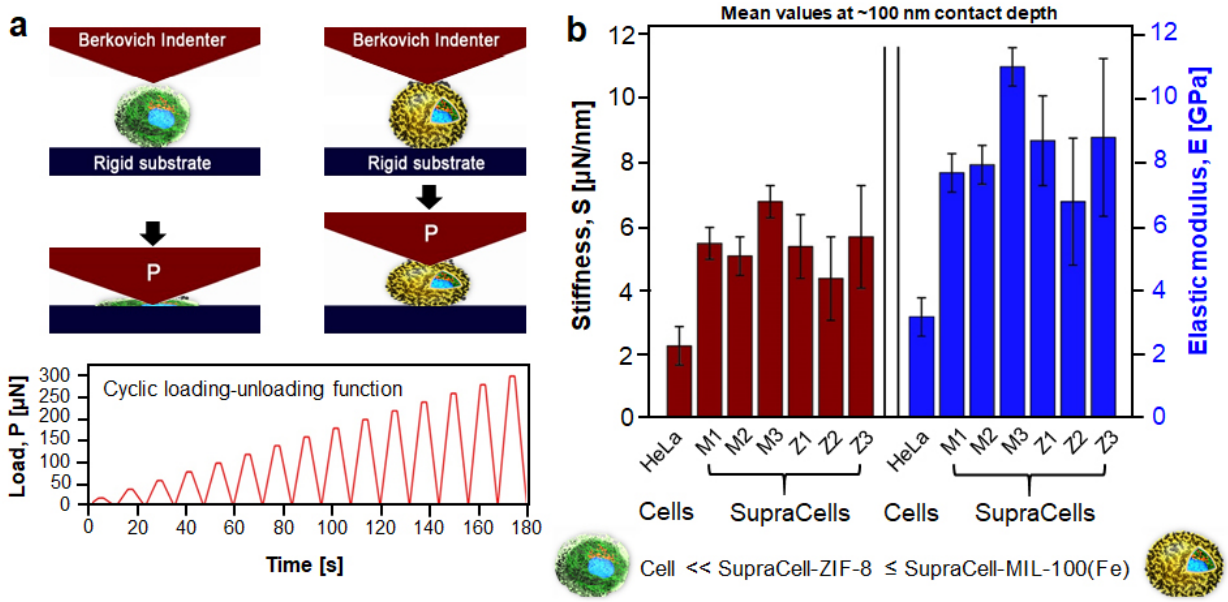

Figure 3. Enhanced mechanical resistance of SupraCells. (**A**) Representation of the mechanical response test set-up involving the Berkovich Indenter imposing a P load onto cells (left) and SupraCells (right) using a cyclic loading-unloading function. This cyclic load function has been selected to ensure that the measurements have not been affected by the surface roughness. (**B**) Stiffness and elastic modulus of HeLa cells and SupraCells-MIL-100(Fe) or ZIF-8 (M or Z refers to MIL-100(Fe) or ZIF-8, respectively); the number 1-3 refers to the coating cycle).

As represented in Figure 4, the SupraCell construct can be extended to a large number of nanoparticle types and combinations to achieve varied functions. A common function of all SupraCells is that the uniform and complete encapsulation with various NPs introduces a non-native, size-selective permeability to the exoskeleton that can maintain viability while serving to protect the cell against certain exogenous toxins and pathogens. To demonstrate the aspects of size selective permeability, SupraCell-MIL-100(Fe) was selected because, as shown in Figure S35, it is composed of two connected mesocage networks that act as molecular sieves preventing transport of entities greater than 2.9 nm in kinetic diameter. First, preservation of the permeability of the Supracell to molecular components was demonstrated using labeled glucose tracers (2-Deoxy-2-[(7-nitro-2,1,3-benzoxadiazol-4-yl)amino]-D-glucose

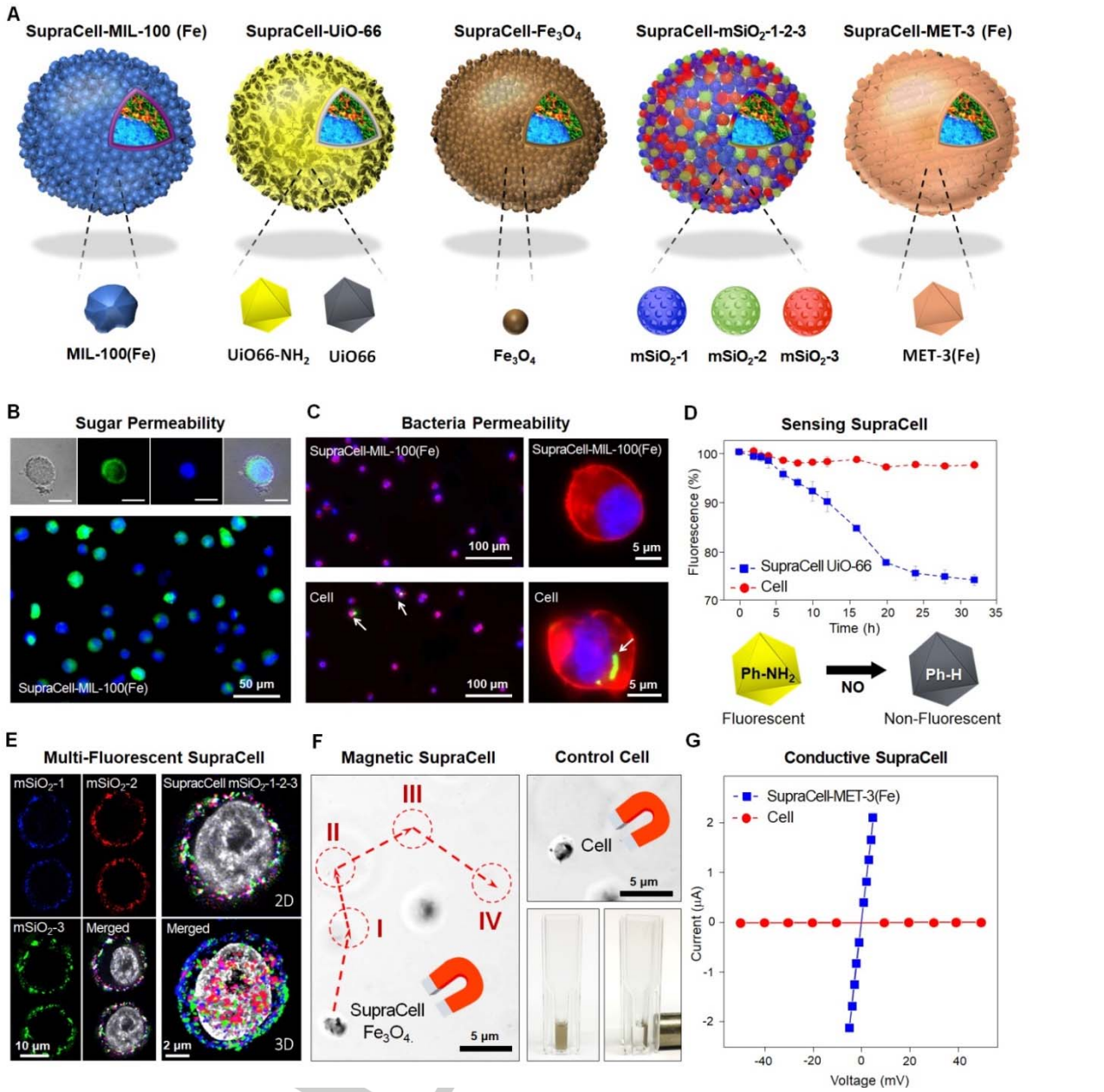

Figure 4. SupraCell-properties based on modular functional NP-based exoskeletons. (**A**) Representation of various SupraCells characterized by one or more nanobuilding block type. (**B-C**) Size-selective permeability studies of SupraCell-MIL-100(Fe) involving (**B**) sugar permeation and (**C**) bacteria non-permeation (confocal images show the intracellular green fluorescence of bacteria only in normal cells). (**D**) Timeline of the fluorescence of cellular NO-sensing SupraCell based on fluorescent UiO-66(Ph-NH_2) nanobuilding blocks upon NO detection. (**E**) Confocal images of multi-fluorescent SupraCell based on three different fluorescent $mSiO_2$ nanobuilding ($mSiO_2$-1-2-3) blocks. (**F**) Bright-field microscopy images of magnetically-actuated SupraCell-Fe_3O_4 (left) or immobile normal cell (top right). Photographs of a dispersion of SupraCells before (left) and after (right) placing a magnet on its side. (**G**) Current-voltage plot demonstrating the conductivity imparted to SupraCells via MET-3 (Fe) MOF NP-based exoskeletons.

(2-NBDG)) (Figure 4B). Then, the anticancer drug doxorubicin (diameter ~1.6 nm) was added into the culture medium at different concentrations. As shown in Figure S36, both native cells and SupraCells were sensitive to doxorubicin and each exhibited a nearly identical dose response curve. Combined with the described results in Figure 2F where native cells but not SupraCells were sensitive to Ag NPs (diameter ~5.0 nm), these results established an effective pore size cut-off of the exoskeleton membrane (> 5 nm) consistent with the pore size of the MIL-100(Fe). The MIL-100(Fe)-based exoskeleton also prevented phagocytosis of GFP-expressing *Salmonella enterica serovar* Typhimurium LT2 bacteria (Figure 4C). SupraCells are thus endowed with a unique semi-permeability allowing nutrient uptake but denying attack by pathogens.

As depicted in Figure 4A the SupraCell concept can be extended generally to other NP types and combinations to achieve diverse functionalities including multifluorescent labeling, sensing, magnetic, and conductive properties (Figure 4D-G), while maintaining >90% viability of all respective SupraCells (Figure S22). As an example, multi-fluorescent SupraCells were fabricated by incubating HeLa cells simultaneously with equal concentrations of three different fluorescently labeled mesoporous silica nanoparticles in a one-pot process for less than one minute (Figure S37). Confocal microscopy images in 2D and 3D demonstrated the formation of a continuous exoskeleton and a homogeneous distribution of MSNs that preserved the stoichiometry of the synthesis solution (Figure 4E). We next designed sensing SupraCells to demonstrate in-situ monitoring of intracellular nitric oxide (NO), which is a key signaling molecule in many pathological processes.[22] NO sensing was achieved using luminescent MOF nanobuilding blocks (UiO-66-NH_2 NPs) whose luminescence is quenched upon NO-triggered de-amination, allowing real time NO detection.[23] Using metal-phenolic linker chemistry, Mouse macrophage Raw 264.7 cells were encapsulated with UiO-66-NH_2 NP-

based exoskeletons as demonstrated by the blue fluorescent coronas observed around the surface of SupraCells (Figure S38). SupraCells were then exposed to lipopolysaccharide (LPS), a traditional exogenous activator of the TLR4 (toll-like receptor 4)-NF-κB-iNOS (inducible nitric oxide synthase) (Figure S39) pathway[24] resulting in time-dependent luminescence quenching indicative of NO detection (Figure 4D). After 32 h incubation, UiO-66-NH_2 SupraCells exposed to LPS exhibited ~25% quenching relative to SupraCells not exposed to LPS that showed no significant quenching.

Magnetic SupraCells that hold great potential as magnetic resonance imaging (MRI) agents and micro-motorized cellular constructs were prepared using ca. 8.0-nm diameter iron oxide (Fe_3O_4) nanobuilding blocks.[25] Using boronate-phenolic linker chemistry, HeLa cells were encapsulated within a continuous magnetic Fe_3O_4 exoskeleton (Figure S19), which allows the movement of cells to be controlled via an external magnetic field (Figure 4F and Video S1). Finally electrically conductive SupraCells were synthesized using electrically conductive metal-triazolate MOF of MET-3(Fe) NPs.[26] As shown in Figure S16, HeLa cells were uniformly encapsulated within MET-3(Fe) exoskeletons. The ohmic conductivity of the SupraCell-MET-3(Fe) was assessed via in-situ SEM electrical characterizations (Figure 4G and Figure S40). By placing the SEM probe onto the SupraCell surfaces, representative current-voltage (IV) curves for SupraCell-MRT-3(Fe) and HeLa cells were reliably obtained (Figure 4G). A high resistivity (~8.75 MΩ) was measured for the native cells, as expected from the non-conductive cell cytoskeletons and intracellular components. In contrast, a dramatic decrease in the resistance by approximately 3600-fold (~2.4 kΩ) was measured for the SupraCell-MRT-3(Fe). Conductive SupraCells thus appear as promising living microdevices for applications in biological fuel cells.

In summary, we have developed a general, simple, and modular approach to create a new class of living hybrid materials termed SupraCells with diverse possible functionalities. Using linker chemistries we encapsulate mammalian cells within nanoparticle-based exoskeleotons in an instantaneous process that avoids/abolishes NP internalization pathways such as phagocytosis. The NP exoskeletons are shown to be continuous and to maintain cell viabilities for a long period of time in a non-replicative state endowed with extremophile-like properties. Metal chelation disrupts the linker chemistry and cells return to their native states. The exoskeletons exhibit size selective permeability protecting the cells against toxins and pathogens exceeding 5-nm in diameter. Potential SupraCell functionalities are as diverse as the NP exoskeleton building blocks themselves. SupraCells demonstrated high viabilities with preserved typical metabolic signatures of the native cells, enhanced resistances against both endogenous and exogenous stressors, and extraordinary properties foreign to native cells based on the nature of the nanobuilding blocks integrated into their unique exoskeletons. The generalized functionalization/modification of mammalian cells with diverse classes of NPs and NP combinations has created new cellular phenotypes whose potential applications include cell-based sensing under extreme conditions, regenerative medicine, immunotherapy, as well as 3D cell printing and tissue engineering.

Acknowledgments

This work was supported by the US Department of Energy, Office of Science, Division of Catalysis Science under Grant No. DE-FG02-02ER15368, the Air Force Office of Scientific Research under Grant No. FA9550-14-1-0066, the National Science Foundation under Cooperative Agreement No. EEC-1647722, and the U.S. Department of Energy's National Nuclear Security Administration under contract DENA-0003525. Part of this work was

conducted and funded by the Australian Research Council (ARC) Centre of Excellence in Convergent Bio-Nano Science and Technology (project number CE140100036). F.C. acknowledges the award of a National Health Medical Research Council Senior Principal Research Fellowship (APP1135806). W. Z. and J. G. contributed equally to this work.

Keywords: mammalian cell • nanoparticles • artificial exoskeleton • biomimetic encapsulation • multifunctions

References

[1] a) Z. Liu, X. Xu, R. Tang, *Adv. Funct. Mater.* **2016**, *12*, 1862; b) J. Yang, J. Li, X. Li, X. Wang, Y. Yang, N. Kawazoe, G. Chen, *Biomaterials* **2017**, *133*, 253; c) J. K. Lee, I. S. Choi, T. I. Oh, E. Lee, *Chem. Eur. J.*, **2018**, *24*, 15725.

[2] a) R. Riccò, K. Liang, S. Li, J. J. Gassensmith, F. Caruso, C. Doonan, P. Falcaro P, *ACS Nano* **2018**, *12*, 13; b) J. H. Park, S. H. Yang, J. Lee, E. H. Ko, D. Hong, I. S. Choi, *Adv. Mater.* **2014**, *26*, 2001; c) W. Geng, L. Wang, N. Jiang, J. Cao, Y. Xiao, H. Wei, A. K. Yetisen, X. Yang, B. Su, *Nanoscale*, **2018**, *10*, 3112; d) N. Jiang, X. Yang, G. Ying, L. Shen, J. Liu, W. Geng, L. Dai, S. Liu, J. Cao, G. Tian, T. Sun, S. Li, B. Su, *Chem. Sci*., **2015**, *6*, 486.

[3] a) K. Kadowaki, M. Matsusaki, M. Akashi, *Langmuir* **2010,** *26*, 5670; b) M. B. Oliveira, J. Hatami, J. F. Mano, *Chem. Asian J*. **2016**, *11*, 1753.

[4] J. Niu, D. J. Lunn, A. Pusuluri, J. I. Yoo, M. A. O'Malley, S. Mitragotri, H. T. Soh, C. J. Hawker, *Nat. Chem*. **2017**, *9*, 537.

[5] a) J. Lee, J. Choi, J. H. Park, M. H. Kim, D. Hong, H. Cho, S. H. Yang, I. S. Choi, *Angew. Chem. Int. Ed*. **2014**, *53*, 8056; *Angew. Chem.* **2014**, *126*, 8194; b) W. Youn, E. H. Ko, M. H. Kim, M. Park, D. Hong, G. A. Seisenbaeva, V. G. Kessler, I. S. Choi, *Angew. Chem. Int. Ed*. **2017**, *56*, 10702; *Angew. Chem.* **2017**, *129*, 10842; c) E. H. Ko, Y. Yoon, J. H. Park, S. H. Yang, D. Hong, K.-B. Lee, H. K. Shon, T. G. Lee, I. S. Choi, *Angew. Chem. Int. Ed*. **2013**, *52*, 12279; *Angew. Chem.* **2013**, *125*, 12505.

[6] a) J. Lee, H. Cho, J. Choi, D. Kim, D. Hong, J. H. Park, S. H. Yang, I. S. Choi, *Nanoscale*, **2015**, *7*, 18918; b) J. H. Park, K. Kim, J. Lee, J. Y. Choi, D. Hong, S. H. Yang, F. Caruso,

Y. Lee, I. S. Choi, *Angew. Chem. Int. Ed*. **2014**, *53*, 12420; *Angew. Chem.* **2014**, *126*, 12628; c) B. J. Kim, S. Han, K.-B. Lee, I. S. Choi, *Adv. Mater*. **2017**, *29*, 1700784.

[7] a) R. Liu, J. Zhao, Q. Han, X. Hu, D. Wang, X. Zhang, P. Yang, *Adv. Mater.* **2018**, *30*, 1802851; b) F. Yang, F. Tao, C. Li, L. Gao, P. Yang, *Nat. Commun.* **2018**, *9*, 5443.

[8] a) J. H. Park, D. Hong, J. Lee, I. S. Choi, *Acc. Chem. Res*. **2016**, *49*, 792; b) J. Guo, B. L. Tardy, A. J. Christofferson, Y. Dai, J. J. Richardson, W. Zhu, M. Hu, Y. Ju, J. Cui, R. R. Dagastine, I. Yarovsky, F. Caruso, *Nat. Nanotech*. **2016**, *11*, 1105; c) Z. Ji, H. Zhang, H. Liu, O. M. Yaghi, P. Yang, *Proc. Natl. Acad. Sci. U.S.A*., **2018**, *115*, 10582.

[9] a) F. Tang, L. Li, D. Chen, *Adv. Mater.* **2012**, **22**, 1504; b) R. Freund, U. Lächelt, T. Gruber, B. Rühle, S. Wuttke, *ACS Nano* **2018**, *12*, 2094; c) C. He, D. Liu, W. Lin, *Chem. Rev*. **2015**, 115, 11079.

[10] a) C. C. Fleischer, C. K. Payne, *Acc. Chem. Res.* **2014**, *47*, 2651; b) A. Verma, F. Stellacci, *Small* **2010**, *6*, 12; c) J. G. Croissant, Y. Fatieiev, N. M. Khashab, *Adv. Mater.* **2017**, **29**, 1604634; d) W. Zhu, J. Guo, Y. Ju, R. E. Serda, J. G. Croissant, J. Shang, E. Coker, J. O. Agola, Q-Z, Zhong, F. Caruso, C. J. Brinker, *Adv. Mater.* **2019**, **31**, 1806774.

[11] a) H. Ejima, J. J. Richardson, K. Liang, J. P. Best, M. P. van Koeverden, G. K. Such, J. Cui, F. Caruso, *Science* **2013**, *341*, 154; b) W. Zhu, G. Xiang, J. Shang, J. Guo, B. Motevalli, P. Durfee, J. O. Agola, E. N. Coker, C. J. Brinker, *Adv. Funct. Mater.* **2018**, *28*, 1705274.

[12] a) K. Liang, J. J. Richardson, J. Cui, F. Caruso, C. J. Doonan, P. Falcaro P, *Adv. Mater.* **2016**, *28*, 7910; b) K. Liang, J. J. Richardson, C. J. Doonan, X. Mulet, Y. Ju, J. Cui, F. Caruso, P. Falcaro, *Angew. Chem. Int. Ed*. **2017**, *56*, 8510; *Angew. Chem.* **2017**, *129*, 8630.

[13] J. Guo, H. Sun, K. Alt, B. L. Tardy, J. J. Richardson, T. Suma, H. Ejima, J. Cui, C. E. Hagemeyer, F. Caruso, *Adv. Healthc. Mater*. **2015**, *4*, 1796.

[14] Y. Jin, C. Yu, R. J. Denman, W. Zhang, *Chem. Soc. Rev*. **2013**, *42*, 6634.

[15] M. C. Guadamillas, C. Ana, A. P. Miguel, *J. Cell. Sci.* 2011, **124**, 3189.

[16] A. Nel, T. Xia, L. Mädler, N. Li, *Science* **2006**, *311*, 622.

[17] C. R. Evans, N. Miller, G. Paganga, *Trends In Plant Science* **1997**, *2*, 152.

[18] S. K. Parks, J. Chiche, J. Pouysségur, *Nat. Rev. Cancer* **2013**, *13*, 611.

[19] a) H. Furukawa, K. E. Cordova, M. O'Keeffe, O. M. Yaghi, *Science* **2013**, *341*, 1230444; b) L. J. Murray, M. Dincă, J. R. Long, *Chem. Soc. Rev.* **2009**, *38*, 1294; c) J. Li, J. Sculley, H. Zhou, *Chem. Rev*. **2012**, *112*, 869.

[20] P. Talalay, J. W. Fahey, Z. R. Healy, S. L. Wehage, A. L. Benedict, C. Min, A. T. Dinkova-Kostova, *Proc. Natl. Acad. Sci. U.S.A*., **2007**, *104*, 17500.

[21] A) P. Horcajada, S. Surblé, C. Serre, D. Hong, Y. Seo, J. Chang, J. Grenèche, I. Margiolaki, G. Férey, *Chem. Commun.* **2007**, 2820; b) P. Horcajada, T. Chalati, C. Serre, B. Gillet, C. Sebrie, T. Batti, J. F. Eubank, D. Heurtaux, P. Clayette, C. Kreuz, J. Chang, Y. K. Hwang, V. Marsaud, P. Bories, L. Cynober, S. Gil, G. Férey, P. Couvreur, R. Gref, *Nat. Mater.*, **2010**, *9*, 172.

[22] S. Jiang S, R. Cheng, X. Wang, T. Xue, Y. Liu, A. Nel, Y. Huang, X. Duan, *Nat. Commun*. **2013**, *4*, 2225.

[23] A. V. Desai, P. Samanta, B. Manna, S. K. Ghosh, *Chem. Commun.* **2015**, *51*, 6111.

[24] V. Toshchakov, B. W. Jones, P. Perera, K. Thomas, M. J. Cody, S. Zhang, B. R. G. Williams, J. Major, T. A. Hamilton, M. J. Fenton, S. N. Vogel, *Nat. Immunol*, **2002**, *3*, 392.

[25] H. Wang, M. Pumera, *Chem. Rev*. **2015**, *115*, 8704.

[26] F. Gándara, F. J. Uribe-Romo, D. K. Britt, H. Furukawa, L. Lei, R. Cheng, X. Duan, M. O'Keeffe, O. M. Yaghi, *Chem. Eur. J.* **2012**, *18*, 10595.

TOC

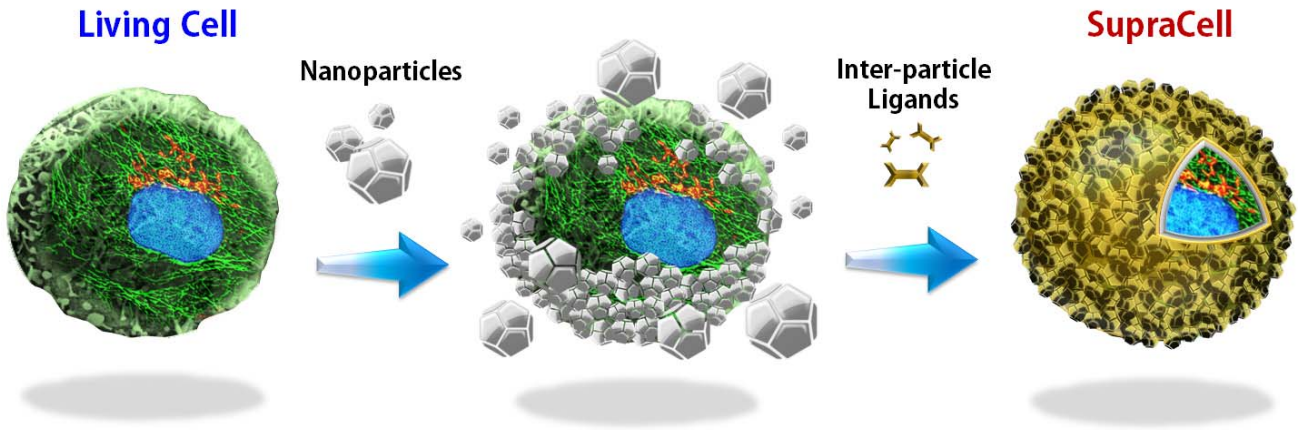

A new concept of 'SupraCells' which are living mammalian cells encapsulated and protected within functional modular nanoparticle-based exoskeletons has been introduced. SupraCell induces a spore-like state, wherein cells do not replicate or spread on surfaces but are endowed with extremophile properties, e.g., resistance to osmotic stress, reactive oxygen species, pH, and UV exposure, along with abiotic properties like magnetism, conductivity, and multi-fluorescence, which are utterly foreign to the native cells.

Author/s:
Zhu, W; Guo, J; Amini, S; Ju, Y; Agola, JO; Zimpel, A; Shang, J; Noureddine, A; Caruso, F; Wuttke, S; Croissant, JG; Brinker, CJ

Title:
SupraCells: Living Mammalian Cells Protected within Functional Modular Nanoparticle-Based Exoskeletons

Date:
2019-06-01

Citation:
Zhu, W., Guo, J., Amini, S., Ju, Y., Agola, J. O., Zimpel, A., Shang, J., Noureddine, A., Caruso, F., Wuttke, S., Croissant, J. G. & Brinker, C. J. (2019). SupraCells: Living Mammalian Cells Protected within Functional Modular Nanoparticle-Based Exoskeletons. ADVANCED MATERIALS, 31 (25), https://doi.org/10.1002/adma.201900545.